Applied Catalysis B: Environmental 129 (2013) 367–374

Contents lists available at SciVerse ScienceDirect

Applied Catalysis B: Environmental

journal homepage: www.elsevier.com/locate/apcatb

Preparation of graphitic mesoporous carbon for the simultaneous detection of hydroquinone and catechol

Xiaoli Yuan[a], Dingsheng Yuan[a,*], Fulong Zeng[a], Wujun Zou[a], Fotini Tzorbatzoglou[b], Panagiotis Tsiakaras[b,*], Yi Wang[c,*]

[a] Department of Chemistry and Institute of Nanochemistry, Jinan University, Guangzhou 510632, China
[b] Department of Mechanical Engineering, School of Engineering, University of Thessaly, Pedion Areos 383 34, Greece
[c] KLGHEI of Environment and Energy Chemistry/The Key Lab of Low-carbon Chemistry & Energy Conservation of Guangdong Province, School of Chemistry and Chemical Engineering, Sun Yat-sen University, Guangzhou 510275, China

ARTICLE INFO

Article history:
Received 24 March 2012
Received in revised form 9 August 2012
Accepted 13 September 2012
Available online 19 September 2012

Keywords:
Graphitic mesoporous carbon
Layered double hydroxides
Simultaneous detection of hydroquinone and catechol

ABSTRACT

A graphitic mesoporous carbon (GMC) had been successfully synthesized using Ni–Fe layered double hydroxide (LDH) as both template and catalyst under a relatively low pyrolysis temperature. The techniques of X-ray diffraction, transmission electron microscopy, Raman spectrum and N_2 adsorption/desorption were used to characterize the physico-chemical properties of the as-prepared GMC. Meanwhile, the voltammetric behaviors of hydroquinone (HQ) and catechol (CC) were studied at the GMC modified glassy carbon electrode (GMC/GCE). The separation of the oxidation and reduction peak (ΔE_p) for HQ and CC were decreased from 369 to 42 mV and from 365 to 52 mV, respectively, and the anodic peak currents for the oxidation of both HQ and CC were also remarkably increased at the GMC/GCE. Furthermore, at the GMC/GCE, the two components could be entirely separated with a large oxidation peak potential separation between HQ and CC. Under the optimized condition, the peak currents of HQ and CC increased linearly with increasing HQ and CC contents. The detection limit for HQ and CC was 3.7×10^{-7} and 3.1×10^{-7} mol L^{-1}, respectively.

1. Introduction

Hydroquinone (HQ) and catechol (CC) are two important isomers of phenolic compounds, which are often used in cosmetics, pesticides, flavoring agents, antioxidant, secondary coloring matters, and photography chemicals [1–3]. Thus, these compounds can be easily introduced into the environment as pollutants during the manufacturing and application process. Meanwhile, most of them are highly toxic to both environment and human even at very low concentrations [4]. Because of their similar structures and properties, it is a challenge to directly and simultaneously determinate the isomers [5–7]. Therefore, it is strongly demanded to develop a highly sensitive and selective analytical method for the simultaneous determination of HQ and CC.

Up to now, several methods such as high performance liquid chromatography (HPLC) [8], spectrophotometry [9], and electro-chemiluminescence [10] have been established for the simultaneous determination of HQ and CC. Compared with the chromatographic and optical methods, electrochemical methods are preferable and attractive for the simultaneous detection of such phenolic compounds due to the advantages of fast response, cheap instrument, low cost, simple operation, time saving, high sensitivity, and excellent selectivity [4,11]. Unfortunately, it cannot be resolved at conventional electrodes such as gold and glassy carbon electrode (GCE) due to the overlapping of the oxidation peak of these two phenolic isomers [9].

In order to address the above problems, many materials have been used to fabricate modified electrodes to achieve their simultaneous voltammetric determination [12,13]. Among them, nanostructured carbon materials with graphitic framework structures have attracted widespread attention for a series of properties such as high electrical conductivity, excellent chemical stability and good field emission performance [14,15]. The unique properties of these carbon materials, primarily in the field of storage and production of energy, provide them with potential applications in many areas [16–18]. Specifically, these nanostructured carbons possess many structural characteristics (i.e., a high crystallinity, a relatively large surface area and an open and accessible porosity), which can meet the requirements for using them directly as catalysts or as the

* Corresponding authors. Tel.: +86 20 85221697; fax: +86 20 85221697 (D. Yuan); Tel.: +30 24210 74065; fax: +30 24210 74050 (P. Tsiakaras); Tel.: +86 20 84110930; fax: +86 20 84110927 (Y. Wang).
E-mail addresses: tydsh@jnu.edu.cn (D. Yuan), tsiak@mie.uth.gr (P. Tsiakaras), wangyi76@mail.sysu.edu.cn (Y. Wang).

0926-3373/$ – see front matter © 2012 Elsevier B.V. All rights reserved.
http://dx.doi.org/10.1016/j.apcatb.2012.09.017

catalyst support materials [19]. According to the above-mentioned points, it can be logically deduced that the nanostructured graphitic carbon material would be a good alternative choice for application in catalysis.

Although graphitic carbon materials possess superior electronic properties and electrochemical performance, the complex methods and severe preparation conditions limit the use of graphitic carbons [20,21]. For instance, the conventional synthetic methods such as electron beam radiation [22], arc discharge [23], and thermal chemical vapor deposition (CVD) [24], which are used to prepare graphitic carbons, require very high temperatures. This makes them costly and complex in terms of scalability [25]. Consequently, developing low-cost and facile synthetic processes have attracted more and more attention. Until present, many researchers have prepared graphitic carbon nanostructures successfully at relatively low temperatures (<1000 °C) in the presence of certain transition metals (Fe, Co, Ni, Mn, etc.) that act as graphitization catalysts [21,26,27]. For example, Sevilla et al. [14] fabricated the graphitic mesoporous carbon materials with silicon aerogel as template and phenolic resin as carbon source respectively by using different catalysts (Fe, Mn, or Ni). Bang [28] developed hollow graphitic carbon spheres by the polymerization of core/shell structured pyrrole micelles followed by carbonization at 900 °C and displayed good electrocatalytic activity. Meanwhile, Zhang et al. [29] also prepared CNTs with low degree of graphitization by catalytic chemical vapor deposition of acetylene using Ni–Mg–Al layered double hydroxides (LDHs) as catalyst.

In this study, graphitic mesoporous carbon (GMC) with high specific surface area has been prepared using Ni–Fe layered double hydroxide (LDH) as both catalyst and template by a simple solid-phase technique under a relatively low pyrolysis temperature. Following this, GMC modified glassy carbon electrode was used to simultaneously detect HQ and CC by using the technique of cyclic voltammetry. Meanwhile, the electrochemical properties of HQ and CC at the GMC modified electrode were also investigated by differential pulse voltammetry. The results demonstrated that two corresponding well-defined oxidation peaks with significantly differing peak potential and enhanced peak currents of HQ and CC appeared at the modified electrode. The GMC prepared with Ni–Fe layered double hydroxide (LDH) has not been reported so far, and it is demonstrated for the first time that the GMC/GCE has been achieved for the simultaneous detection of HQ and CC with high sensitivity.

2. Experimental

2.1. Preparation of graphitic mesoporous carbon (GMC)

Ni–Fe layered double hydroxide (LDH) (molar ratio of $Ni^{2+}/Fe^{3+} = 2$) was synthesized according to the previous report [30]. Typically, $Ni(NO_3)_2{\cdot}6H_2O$ and $Fe(NO_3)_3{\cdot}9H_2O$ with a molar ratio of 2 were dissolved in 200.0 mL deionized water to form solution A. Solution B was prepared by dissolving sodium hydroxide (0.5 mol) and sodium carbonate (0.2 mol) in 200.0 mL deionized water. Then, the above two solutions were added dropwise to a beaker, containing 100.0 mL of deionized water under stirring at 303 K. After about 3.5–4 h, to complete the addition, the precipitates were aged at 338 K for 18 h in a thermostatic bath. The Ni–Fe LDH was obtained by filtering and washing thoroughly with warm deionized water until the filtrate showed no presence of NaOH and subsequently was dried at 373 K overnight.

The graphitic mesoporous carbon was prepared as follows: 0.9 g sucrose was dissolved in a 15 mL beaker containing 8.0 mL deionized water. The as-prepared Ni–Fe LDH (0.5 g) was added into sucrose solution accompanied with continuous stirring for 1 h to get a mixture. After covered with taut saran wrap, the beaker was put in the oven at 100 °C for 6 h, and then the saran wrap was deserted. Following this, the reaction condition was adjusted to 160 °C and kept at this temperature for 6 h. The precipitate was dried and pyrolyzed at 900 °C for 4 h under nitrogen flow. Finally, the Ni–Fe LDH was removed by immersing in 3.0 mol L^{-1} HCl solution at 80 °C for 24 h, followed by washing with copious deionized water and drying in oven at 60 °C. The as-obtained graphitic carbon product was denoted as GMC.

2.2. Physical characterization

The structure of the GMC was analyzed by a MSALXD2 X-ray diffractometer ($Cu_{K\alpha}$, 36 kV, 20 mA, and $\lambda = 1.54056$ Å). The morphology was observed via a Philips TECNAI-10 transmission electron microscope (TEM) using an accelerating voltage of 100 kV and JEM2010 high-resolution transmission electron microscopy (HRTEM) operating at 200 kV. The degree of crystalline structure of GMC was investigated by a Raman spectroscopy, which was recorded in a backscattering configuration using the 514.5 nm line of an Ar^+ ion laser and a Renishaw in Via Plus Raman spectrometer.

2.3. Preparation of the GMC (graphitic mesoporous carbon) modified electrode

Before surface modification, the bare glassy carbon electrodes (GCE) (4.0 mm in diameter) were polished to a mirror-like with 0.05 μm alumina/water slurry on a polishing cloth, rinsed thoroughly with ethanol and double-deionized water and dried in high-purity nitrogen blow. The detailed process for the preparation of the modified electrode was as follows: 3.0 mg of the as-prepared GMC was dispersed in 3.0 mL N,N-dimethylformamide (DMF) and Nafion solution (0.5 wt%) under ultrasonic condition for 1 h to obtain a 1.0 mg mL^{-1} black suspension, then 10 μL of GMC suspension was dropped onto the surface of the pretreated GCE (glassy carbon electrode). The solvent was dried under an infrared lamp to obtain the GMC/GCE.

2.4. Electrochemical measurements

Electrochemical experiments were carried out using a CHI 660D Electrochemical Analyzer in a conventional three-electrode cell. The working electrode was a GCE (4.0 mm in diameter) or the modified electrode, a platinum foil and an Ag/AgCl electrode (in saturated KCl solution) was served as the counter electrode and the reference electrode, respectively. High-purity nitrogen was used for evacuating oxygen before each experiment. It should be noted that without specification, all the potentials are referred to the Ag/AgCl (in saturated KCl solution). The electrochemical performance of GMC was measured by the cyclic voltammetry (CV) and the different pulse voltammetry (DPV).

3. Results and discussion

3.1. Physical characterization

As shown in Fig. 1, the XRD patterns of the Ni–Fe LDH sample are similar to the reported diagram [31]. The interlayer distance d in LDH can be calculated using Bragg's equation:

$$n\lambda = 2d \sin\theta \quad (1)$$

where n is the order of reflection [equal to 1 for (0 0 3)], λ is the wave length of $Cu_{K\alpha}$ radiation, and θ is the half of the scattering angle [32]. The calculated result shows that the intercalated LDH possesses a basal spacing of 0.77 nm. The characteristic diffraction peaks at low 2θ values are ascribed to the planes of (0 0 3),

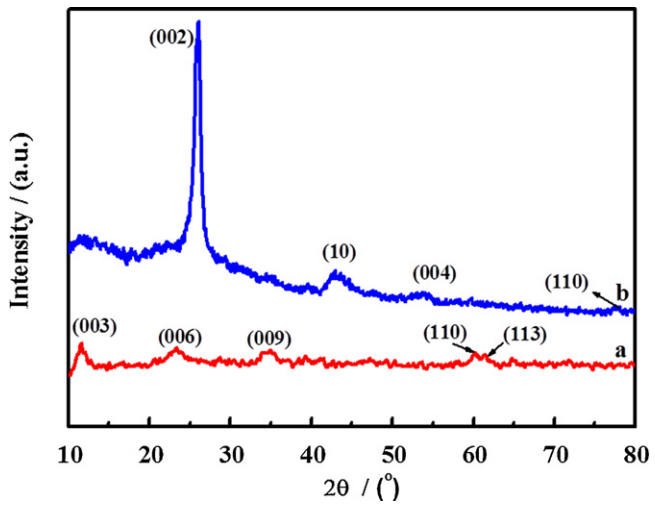

Fig. 1. XRD patterns of Ni–Fe LDH (a) and graphitic mesoporous carbon (b).

(0 0 6) and (0 0 9) corresponding to the basal spacing and higher order diffractions of LDH, indicating that the LDH is typical HT-like LDH material [33]. Moreover, Fig. 1 depicts the XRD pattern of the graphitic mesoporous carbon. The results exhibit the well-resolved diffraction peaks at 26°, 43°, 53° and 78°, which can be assigned to the (0 0 2), (1 0), (0 0 4) and (1 1 0) planes of the graphitic framework, respectively. The sharp and narrow (0 0 2) diffraction plane of the GMC is associated with a high graphitic character [34]. The d_{002} spacing value of the GMC is measured about 0.34 nm, suggesting that the sample synthesized with Ni–Fe LDH is graphitic carbon with high crystallinity. Therefore, it can be known that the highly graphitic mesoporous carbon can be successfully prepared using Ni–Fe LDH as both catalyst source and template.

The graphitic characteristic of GMC is further confirmed by Raman spectroscopy (Fig. 2). The material exhibits two distinct peaks at about 1350 cm^{-1} (D-band) and 1580 cm^{-1} (G-band). In addition, a peak at 2709 cm^{-1} (2D-band) was clearly observed in GMC, which can be observed only in highly-developed graphitic carbon [35]. The G-band is related to the vibration of sp^2 bonded carbon atoms in a two-dimensional hexagonal lattice, which often relates to the formation of ordered graphite layers. The D-band is often referred to the "disorder" band, which results from the imperfection or loss of hexagonal symmetry of the graphite structure

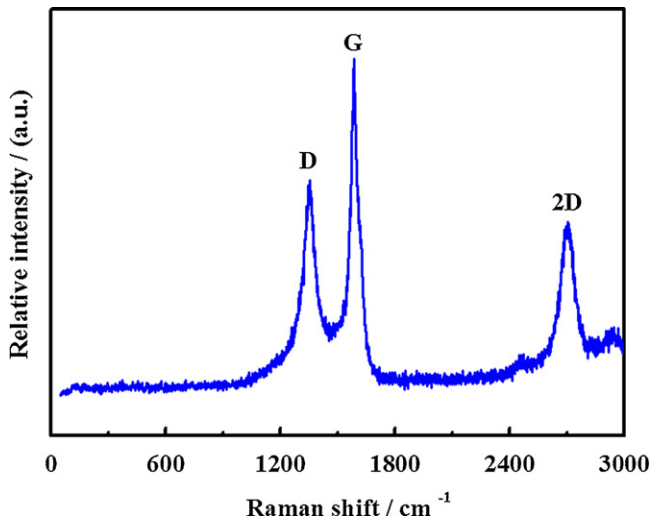

Fig. 2. Raman spectrum of the graphitic mesoporous carbon.

[36]. It is known that the relative intensity ratio between the D and G bands (I_D/I_G) reflect the degree of graphitization. Accordingly, the low I_D/I_G value indicates a high degree of graphitization [37]. The I_D/I_G value of GMC is 0.66, suggesting that the GMC has highly graphitic characteristic with high degree of graphite ordering. Fig. 3 shows the TEM and HRTEM images of the graphitic mesoporous carbon. It can be observed that GMC exhibits carbon nanocages with the porous structure (see Fig. 3A). An enlarged TEM image from B area of Fig. 3A is shown in Fig. 3B, presenting the detailed structure characteristics such as mesopores, micropores graphitic structure and amorphous carbon. To further reveal fine morphology, Fig. 3C and D shows HRTEM images of C and D areas in Fig. 3B. The fringe of the graphite crystallite and layered ribbon-like graphitic structure are distinctly presented in Fig. 3C. The interlayer spacing is measured and found to be ca. 0.34 nm, which are perfectly corresponding to the (0 0 2) distance of graphitic carbon lattice. Some worm-like mesopores and micropores can be found, as shown in Fig. 3D, resulting from the removal of the LDH nanoparticles distributed inside the carbon matrix. This result is in accordance with the above XRD and Raman analysis.

The Brunauer–Emmett–Teller (BET) surface area and the pore structure of Ni–Fe LDH and graphitic carbon material are examined via nitrogen adsorption–desorption measurement and the results are shown in Fig. 4. The isotherm of LDH possesses the characteristic type-IV shape with type H1 hysteresis loops defined by IUPAC [38]. This suggests that it is plate-like particles. The LDH is predominantly mesoporous in the range of 3.8–4.8 nm and the surface area is 168 $m^2\ g^{-1}$ with a pore volume 0.11 $cm^3\ g^{-1}$. A type IV isotherm with H2 hysteresis loop is found on the graphitic mesoporous carbon material, as shown in Fig. 4B. The surface area and pore size of GMC are 178 $m^2\ g^{-1}$ and 9.1 nm, respectively, which are higher than that of the LDH template.

3.2. Electrochemical experiments

3.2.1. Electrochemical behavior of HQ and CC at GMC modified GCE

The electrochemical behaviors of HQ and CC were carefully investigated at the bare GCE and GMC/GCE using cyclic voltammetry. The electrochemical responses obtained on the bare GCE and the GMC/GCE in 0.10 mol L^{-1} PBS solution (pH 3.0) with 5×10^{-5} mol L^{-1} HQ (A) and 5×10^{-5} mol L^{-1} CC (B) are given in Fig. 5. At the bare GCE (curve a), the oxidation peak potential and the reduction peak of HQ and CC appear at about 0.501/0.132 and 0.598/0.233 V, respectively. The respective large peak potential separation (ΔE_p) for HQ and CC are 369 and 365 mV, indicating that HQ and CC exhibit an irreversible electrochemical behavior at bare GCE [4,5]. In contrast, at GMC/GCE (curve b), the anodic and cathodic peaks for HQ and CC are 0.325/0.283 and 0.436/0.384 V, respectively. The dramatically reduced ΔE_p of only 42 and 52 mV for HQ and CC manifests the fast electron transfer between HQ (or CC) and electrode due to the presence of GMC. In addition, the peak currents also increase about six-fold at the GMC/GCE. The results indicate that the GMC modified electrode lowers the oxidation overpotential of HQ and CC, and thus greatly improved electrochemical reversibility of HQ and CC.

Fig. 6 depicts the CVs and DPVs obtained for the mixture of 5×10^{-5} mol L^{-1} HQ and 5×10^{-5} mol L^{-1} CC at bare GCE and GMC/GCE at a scan rate of 20 mV s^{-1} in 0.1 mol L^{-1} PBS solution (pH 3.0). At the bare GC electrode, there is a broad oxidation peak at 0.551 V owing to the overlap of the oxidation peaks of HQ and CC, and two-reduction peaks at 0.160 and 0.266 V, corresponding to the reduction of HQ and CC, respectively. It indicates that the oxidation of HQ and CC at the bare GCE is irreversible and electron transfer kinetics is sluggish. Therefore, it is impossible to

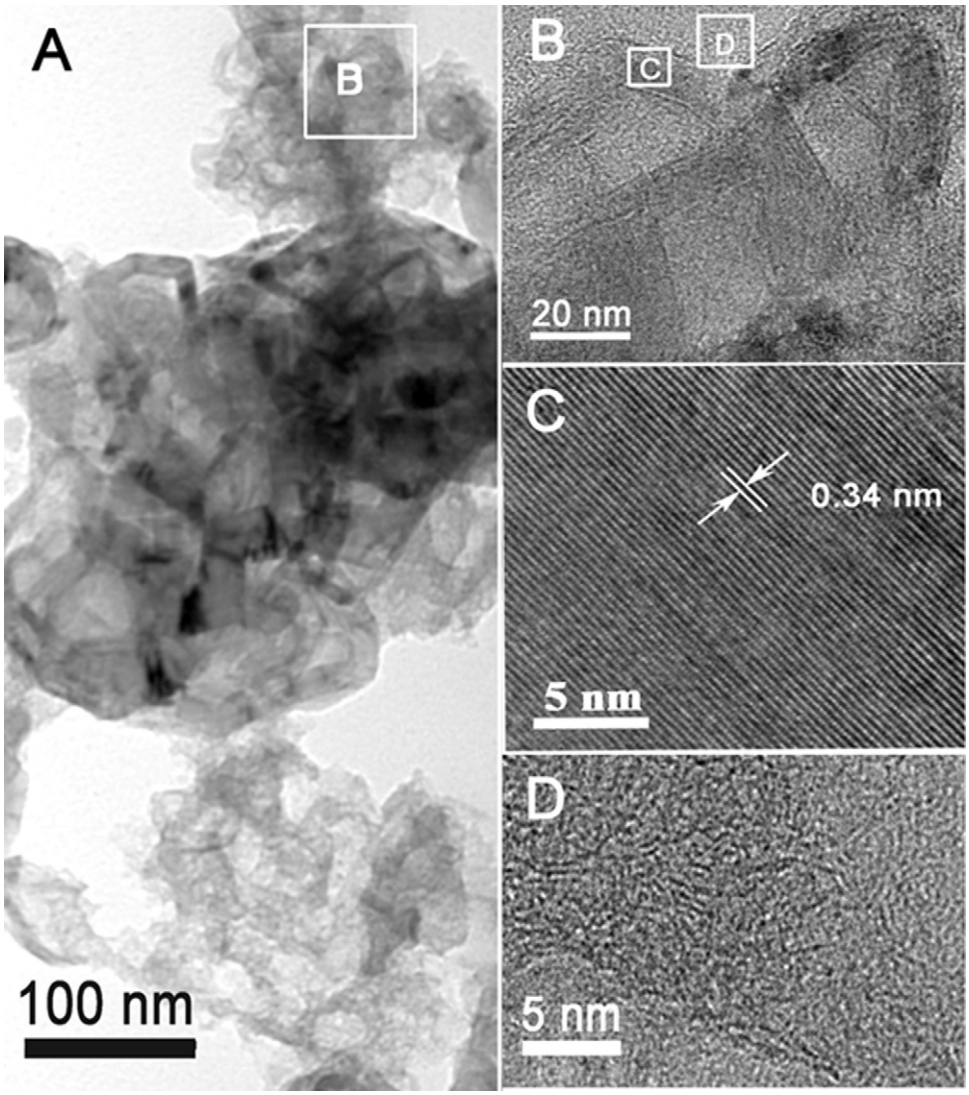

Fig. 3. TEM and HRTEM images of the graphitic mesoporous carbon.

separate HQ and CC from each other by voltammetric determination at the bare GCE. However, at the GMC/GCE, two pairs of well-defined oxidation peaks of HQ and CC appear at 0.323/0.281 and 0.426/0.391 V, and the separation of anodic and cathodic peak potentials (ΔE_p) are 42 mV and 35 mV, respectively. The smaller values of ΔE_p indicate that the oxidation overpotential of HQ and CC are significantly lowered and fast electron-transfer kinetics occurs at the GMC/GCE. Moreover, the anodic peak currents remarkably increase and the separation of oxidation peaks between HQ and CC arrives at about 103 mV, which is large enough to separate the two components. As shown in Fig. 6B, DPV has much higher current sensitivity and better resolution

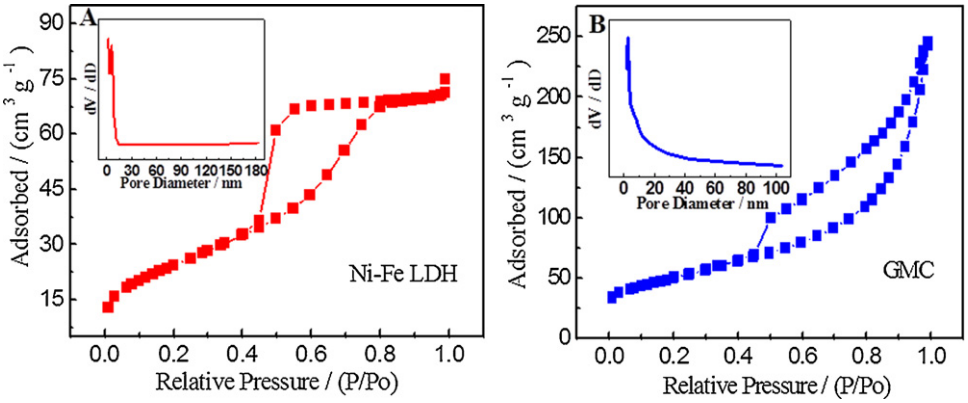

Fig. 4. N_2 adsorption–desorption isotherms of (a) Ni–Fe LDH and (b) graphitic mesoporous carbon.

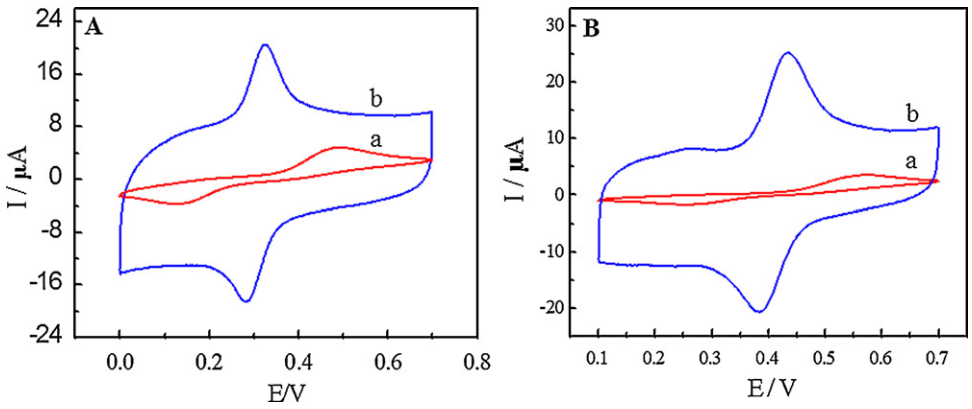

Fig. 5. Cyclic voltammograms at a scan rate of 50 mV s^{-1} for 5×10^{-5} mol L^{-1} HQ (A) 5×10^{-5} mol L^{-1} CC (B) at bare GC (a) and the GMC/GC (b) electrodes in 0.1 mol L^{-1} PBS (pH = 3.0).

than CV, thus DPV is used for the determination of HQ and CC.

The good electrocatalytic response of dihydroxybenzenes at the GMC/GCE may be caused by the following reasons. Firstly, a large number of exposure edge plane defect sites at the surface of GMC may attribute to a large peak current and low oxidation overpotential through providing many active sites to accelerate electron transfer between the electrode and electrolyte [39,40]. Secondly, different space resistances to the different dihydroxybenzenes and the high electron-transfer kinetics of the GMC/GCE are favorable for the separation of HQ and CC during the voltammetry [2]. Thirdly, the GMC possesses two natures: the porous structure (large surface area) and graphitic structure (π–π interactions, conductivity). The GMC with large surface area can adsorb molecules to enhance the regional concentration of the molecules and the graphitic structure offers an electron-rich substrate for electron transfer during the surface reactions, which have great advantages in surface chemistry, especially in catalysis [41]. In addition, the electron cloud density of HQ is lower than CC, so HQ is easier to be oxidized than CC. Therefore, different oxidation–reduction potentials of the dihydroxybenzenes can be observed at the GMC modified electrode interface.

3.2.2. Effect of scan rate on the electrochemical properties of the GMC/GCE

In order to further investigate the electrochemical behaviors of HQ and CC at the modified electrode, the effect of the scan rate on the electrochemical behavior of 5×10^{-5} mol L^{-1} HQ and 5×10^{-5} mol L^{-1} CC was studied on the GMC/GCE by cyclic voltammetry. As shown in Fig. 7, the oxidation peak currents of HQ and CC at the GMC/GCE are directly proportional to the scan rates, indicating that the electrode reaction of HQ and CC is surface controlled redox process rather than a diffusion-controlled process. The linear equations for HQ and CC are obtained as represented in Eqs. (2) and (3), respectively.

$$I_{pa} = 23.05 + 236.9\nu \quad (R = 0.9989) \tag{2}$$

$$I_{pa} = 27.55 + 273.5\nu \quad (R = 0.9990) \tag{3}$$

where I_{pa} is the anodic peak current in μA and ν is the potential scanning rate in the unit of V s^{-1} and R is a correlation coefficient. Moreover, E_{pa} is shifted to more positive values along with scan rates increasing, which suggests that the electron transfer is quasi-reversible [42].

3.2.3. Effect of pH value on the electrochemical properties of the GMC/GCE

The acidity of electrolyte has a significant effect on the HQ and CC electro-oxidation because protons participate in the electrode reaction [43]. Effect of pH values on the peak potentials and the peak currents of HQ and CC at GMC/GCE were carefully investigated by DPV over a pH range of 2.0–7.3, as shown in Fig. 8. It is noticeable that as pH value increases, the peak currents of CC sharply increase until the pH value reaches 3.0, and then decrease. In the case of HQ, a big peak current is also kept at pH 3.0. Afterwards, the peak currents of CC and HQ both gradually decrease with the increase of pH values, which could be caused by the shortage of protons at higher pH value. Moreover, in high pH solution, HQ and CC are easily turned into anions, resulting in the electrostatic repulsion between

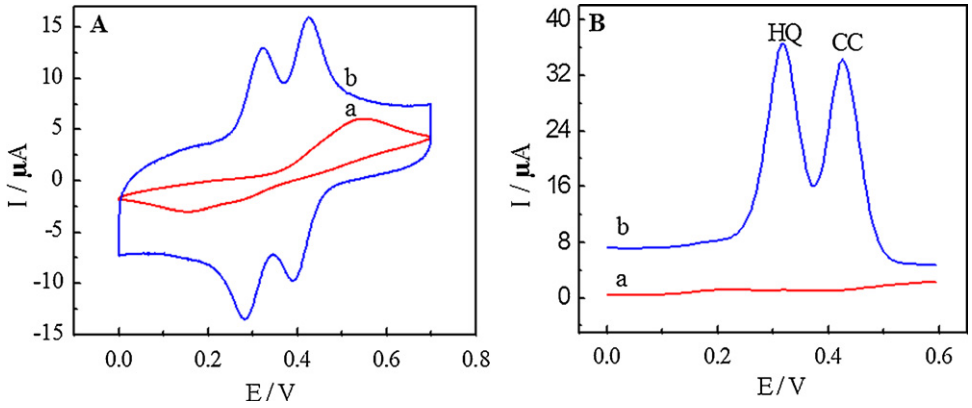

Fig. 6. Cyclic voltammograms (A) and differential pulse voltammograms (B) of 5×10^{-5} mol L^{-1} HQ and 5×10^{-5} mol L^{-1} CC in 0.1 mol L^{-1} PBS (pH = 3.0) solution at the bare GC (a) and the GMC/GC (b) electrodes. DPV conditions: potential incremental, 5 mV; amplitude, 50 mV; pulse width, 50 mV; period, 75 ms.

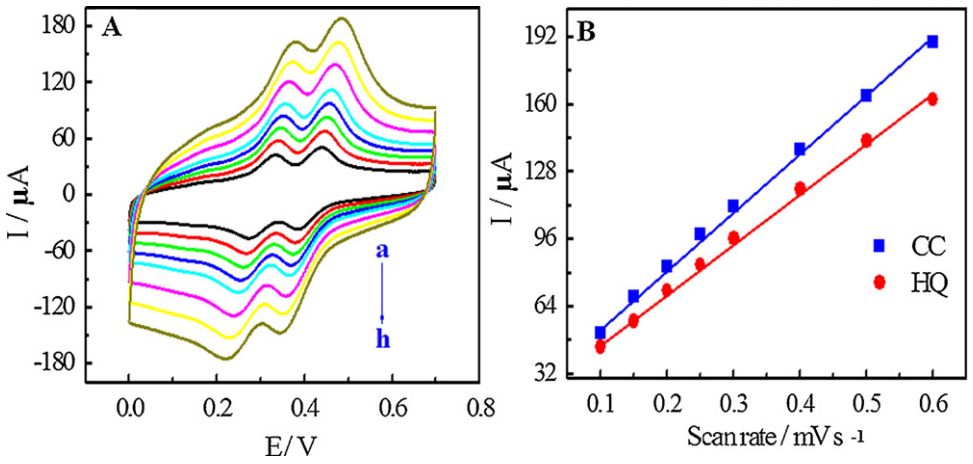

Fig. 7. Effect of scan rate on the redox behavior of 5×10^{-5} mol L^{-1} HQ and 5×10^{-5} mol L^{-1} CC in pH 3.0 PBS at GMC/GCE (A) scan rate: 100, 150, 200, 250, 300, 400, 500, and 600 mV s^{-1}; (B) plot of peak current density versus scan rates (ν: 100–600 mV s^{-1}) for HQ and CC.

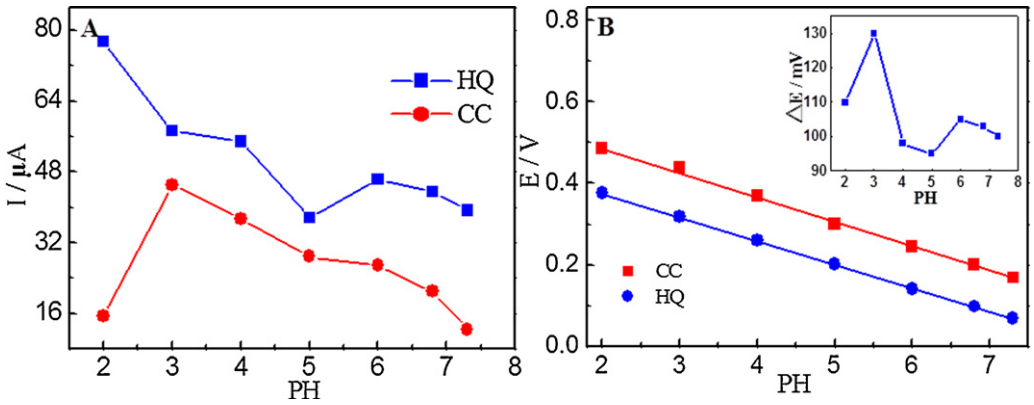

Fig. 8. Effect of pH value on the anodic peak currents (A) and anodic peak potentials (B) of 5×10^{-5} mol L^{-1} HQ and 5×10^{-5} mol L^{-1} CC in 0.1 mol L^{-1} PBS solution at the GMC/GCE. The inset is the separation of the peak potentials ΔE_p. DPV conditions: potential incremental, 5 mV; amplitude, 50 mV; pulse width, 50 mV; period, 75 ms.

the two dihydroxybenzene isomers and the GMC, which may be another reason leading to the decreased peak current values [2].

Fig. 8B shows the relationship between the pH values and the anodic peak potentials of the HQ and CC. With the increase of pH values, the peak potentials of HQ and CC are shifted almost linearly to more negative values, indicating that the protons are directly involved in the electrochemical redox process [44]. The linear regression equations are expressed in Eqs. (4) and (5) for HQ and CC, respectively.

$$E_{pa} = 0.5145 - 0.0619\text{pH} \quad (R = 0.9997) \tag{4}$$

$$E_{pa} = 0.6100 - 0.0600\text{pH} \quad (R = 0.9998) \tag{5}$$

where E_{pa} is the anodic peak potential in V and pH is the corresponding pH value of the solution and R is a correlation coefficient. The peak potentials for HQ and CC show a linear variation with a slope of about 60 mV pH^{-1}, suggesting that two protons are involved in the redox reactions of HQ and CC [45]. Base on the above results, the possible reaction mechanisms of HQ and CC at the GMC/GCE are proposed, as shown in Scheme 1 [2]. In addition, the inset of Fig. 8B shows that the maximum separation of peak potentials for HQ and CC are observed at pH 3.0. Therefore, in order to obtain high sensitivity and good selectivity, pH 3.0 was chosen as an optimum pH value for the electrochemical detection of HQ and CC.

3.3. Simultaneous determination of HQ and CC

DPV possesses higher current sensitivity and better resolution than CV, so it is adopted for the simultaneous determination of HQ and CC at the GMC/GCE. Under the optimized conditions, DPVs of HQ from 2×10^{-6} mol L^{-1} to 5×10^{-5} mol L^{-1} in the presence of 5×10^{-5} mol L^{-1} CC are shown in Fig. 9A. It can be seen that the peak currents of HQ are linear to the concentration of HQ in the two

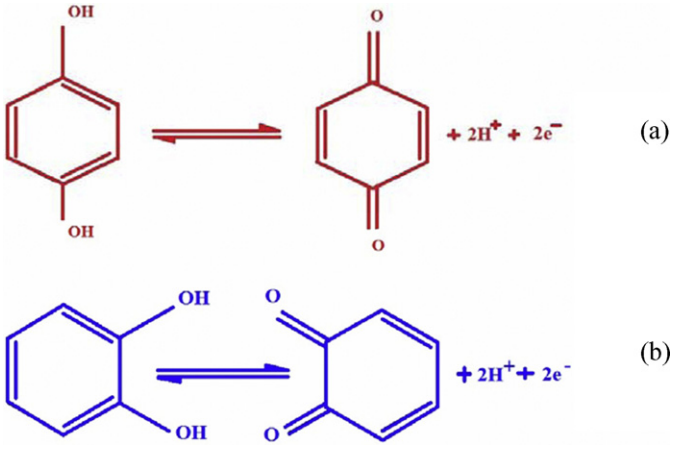

Scheme 1.

Table 1
Performance comparison of the fabricated electrode for HQ and CC detection with other electrodes.

Electrode[a]	Technique	Linear range (10^{-6} mol L^{-1})		Detection limit (10^{-6} mol L^{-1})		Reference
		HQ	CC	HQ	CC	
PPABA/GCE	DPV	1.2–600	2–900	0.4	0.5	[5]
Pen/GCE	DPV	15–115	25–175	1.0	0.6	[6]
PASA/MWNTs/GCE	DPV	6–100	6–180	1.0	1.0	[7]
Graphene-chitosan/GCE	DPV	1–300	1–400	0.75	0.75	[11]
MWNTs/GCE	DPV	1–100	0.6–100	0.75	0.2	[45]
LDHf/GCE	DPV	12–800	3–1500	9.0	1.2	[46]
GMC/GCE	DPV	2–50	2–70	0.37	0.31	This work

[a] LDHF: Zn/Al layered double hydroxide film; PASA: poly-amidosulfonic acid; Pen: penicillamine; MWNTs: multi-wall carbon nanotubes; PPABA: poly(p-aminobenzoic acid); IL-CPE: ionic liquid modified carbon paste electrode.

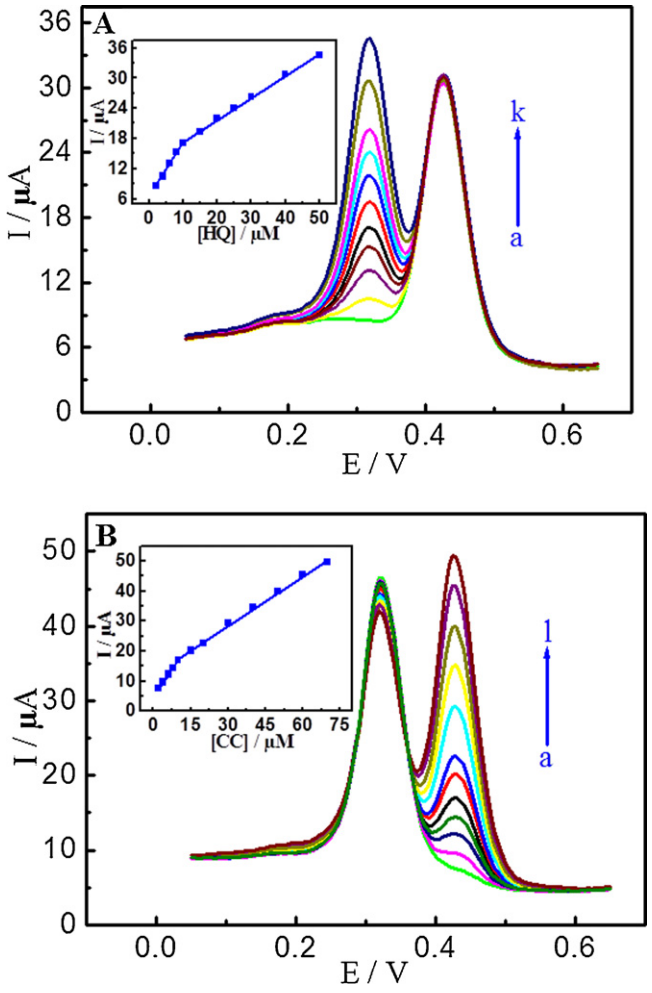

Fig. 9. DPVs obtained at the GMC/GCE in 0.1 mol L^{-1} PBS solution (pH 3.0). (A) a–k: 2.0×10^{-6}, 4.0×10^{-6}, 6.0×10^{-6}, 8.0×10^{-6}, 1.0×10^{-5}, 1.5×10^{-5}, 2.0×10^{-5}, 2.5×10^{-5}, 3.0×10^{-5}, 4.0×10^{-5}, and 5.0×10^{-5} mol L^{-1} of HQ in the presence of 5×10^{-5} mol L^{-1} CC. Insert: calibration plots of HQ. (B) a–l: 2.0×10^{-6}, 4.0×10^{-6}, 6.0×10^{-6}, 8.0×10^{-6}, 1.0×10^{-5}, 1.5×10^{-5}, 2×10^{-5}, 3×10^{-5}, 4×10^{-5}, 5×10^{-5}, 6.0×10^{-5}, and 7.0×10^{-5} mol L^{-1} of CC in the presence of 5×10^{-5} mol L^{-1} HQ. Insert: calibration plots of CC.

concentration intervals. The respective two concentration intervals are 2×10^{-6}–1.0×10^{-5} and 1.0×10^{-5}–5.0×10^{-5} mol L^{-1}. The corresponding linear regression equations in the above two different concentration intervals are expressed in Eqs. (6) and (7).

$$I_{pa} = 6.372 + 1.091c \quad (R = 0.9983) \tag{6}$$

$$I_{pa} = 12.96 + 0.4390c \quad (R = 0.9992) \tag{7}$$

where I_{pa} is the anodic peak current in μA and c is the concentration of HQ in the unit of μmol L^{-1}.The corresponding slopes of the above equations (sensitivity) are 1.091 and 0.4390 μA μmol L^{-1}, respectively. The detection limit is 3.7×10^{-7} mol L^{-1} with a signal-to-noise ratio (S/N) of 3. Similarly, as shown in Fig. 9B, the anodic peak currents of CC increases linearly to the CC concentration over two concentration intervals of 2×10^{-6}–1.0×10^{-5} and 1.0×10^{-5}–7.0×10^{-5} mol L^{-1}. The corresponding linear regression equations are given in Eqs. (8) and (9).

$$I_{pa} = 5.175 + 1.170c \quad (R = 0.9993) \tag{8}$$

$$I_{pa} = 11.99 + 0.5527c \quad (R = 0.9987) \tag{9}$$

where I_{pa} is the anodic peak current in μA and c is the concentration of CC in the unit of μmol L^{-1}.The slopes of the above equation are 1.170 and 0.5527 μA μM^{-1}, and the detection limit is 3.1×10^{-7} mol L^{-1} (S/N = 3). Thus, this proposed method allows the simultaneous and sensitive determination of HQ and CC without interference each other. Meanwhile, a comparison of the proposed method for determination of HQ and CC at other modified electrodes is listed in Table 1. It can be seen that the sensitivity of the proposed method is higher in comparison with some reported electrochemical methods.

3.4. Reproducibility, stability, and interference of GMC/GCE

Under the optimized conditions, the relative standard deviation (RSD %) of the modified electrode in successive eight scans for HQ and CC are 0.33% and 0.12%, respectively. Eight GMC/GCEs were prepared independently under the same conditions, revealing an acceptable reproducibility with the RSD 2.0% and 2.98% for HQ and CC. Finally, the stability of the modified electrode was also examined by storing it in a place at 4 °C for two weeks. The peak current remained 93.1% of the originally measured value. These results confirm the excellent reproducibility and stability of the GMC/GCE.

The possible interferences of some species on the simultaneous determination of HQ and CC were studied by DPV. The results showed that there are no significant interference from many common cations and anions such as Ca^{2+}, Ni^{2+}, Ac^{-}, Zn^{2+}, Cl^{-}, SO_4^{2-}, K^{+}, Na^{+} (each of $c = 1\times10^{-2}$ mol L^{-1}), with signal deviations below 5%. Moreover, a certain concentration of phenol and resorcinol do not cause any interference with the quantitative detection of HQ and CC.

4. Conclusions

Graphitic mesoporous carbon (GMC) with high specific surface area was successfully prepared by a simple solid-phase technique under a relatively low pyrolysis temperature. GMC modified GC electrode was developed for the simultaneous determination of HQ and CC by using CV and DPV. Well-defined oxidation peaks with lower anodic overpotential and the significantly increased

peak current of HQ and CC were observed at the GMC/GC electrode, which is attributed to the large specific surface area and large number of exposure edge plane defect sites at the surface of GMC. At the GMC/GC electrode, HQ and CC exhibited two well-distinguished anodic peaks, indicating that simultaneous determination of HQ and CC was possible. Moreover, the GMC modified electrode also presented lower detection limit. Based on the obtained results, it is evident that the GMC has great potential for isomers determination.

Acknowledgements

This work was supported by National Natural Science Foundation of China (21031001, 20876067 and 21107145) and the Fundamental Research Funds for the Central Universities (21609203) and the grant by Zhujiang Science & Technology New Star of Guangzhou (No. 2011006). This research has been co-financed by the European Union (European Social Fund – ESF) and Greek national funds through the Operational Program "Education and Lifelong Learning" of the National Strategic Reference Framework (NSRF) – Research Funding Program: Heracleitus II. Investing in knowledge society through the European Social Fund.

References

[1] J. Wang, J.N. Park, X.Y. Wei, C.W. Lee, Chemical Communications 5 (2003) 628–629.
[2] H.J. Du, J.S. Ye, J.Q. Zhang, X.D. Huang, C.Z. Yu, Journal of Electroanalytical Chemistry 650 (2011) 209–213.
[3] H. Zhang, J.S. Zhao, H.T. Liu, R.M. Liu, H.S. Wang, J.F. Liu, Microchimica Acta 169 (2010) 277–282.
[4] A.J.S. Ahammad, S. Sarker, M.A. Rahman, J.J. Lee, Journal of Electroanalytical Chemistry 22 (6) (2010) 694–700.
[5] P. Yang, Q.Y. Zhu, Y.H. Chen, F.W. Wang, Journal of Applied Polymer Science 113 (2009) 2881–2886.
[6] L. Wang, P.F. Huang, J.Y. Bai, H.J. Wang, L.Y. Zhang, Y.Q. Zhao, Microchimica Acta 158 (2007) 151–157.
[7] D.M. Zhao, X.H. Liu, X.H. Zhang, J.L. Feng, L. Jia, S.F. Wang, Colloids and Surfaces B 74 (2009) 317–321.
[8] G. Marrubini, E. Calleri, T. Coccini, A.F. Castoldi, L. Manzo, Chromatographia 62 (2005) 25–31.
[9] P. Nagaraja, R.A. Vasantha, K.R. Sunitha, Journal of Pharmaceutical and Biomedical Analysis 25 (2001) 417–424.
[10] Y.G. Sun, H. Cui, Y.H. Li, X.Q. Lin, Talanta 53 (2000) 661–666.
[11] H.S. Yin, Q.M. Zhang, Y.L. Zhou, Q. Ma, T. Liu, L.S. Zhu, S.Y. Ai, Electrochimica Acta 56 (2011) 2748–2753.
[12] Z.M. Liu, Z.L. Wang, Y.Y. Cao, Y.F. Jing, Y.L. Liu, Sensors and Actuators B: Chemical 157 (2011) 540–546.
[13] L.Y. Chen, Y.H. Tang, K. Wang, C.B. Liu, S.L. Luo, Electrochemistry Communications 13 (2011) 133–137.
[14] M. Sevilla, A.B. Fuertes, Carbon 44 (2006) 468–474.
[15] S. Zhang, Y.Y. Shao, G.P. Yin, Y.H. Lin, Applied Catalysis B: Environmental 102 (2011) 372–377.
[16] P. Hernández-Fernández, M. Montiel, P. Ocóna, J.L. Gómez de la Fuente, S. García-Rodríguez, S. Rojas, J.L.G. Fierro, Applied Catalysis B: Environmental 99 (2010) 343–352.
[17] R. Strobel, J. Garche, P.T. Moseley, L. Jorissen, G. Wolf, Journal of Power Sources 159 (2006) 781–801.
[18] S.H. Joo, S.J. Choi, I. Oh, J. Kwak, Z. Liu, O. Terasaki, R. Ryoo, Nature 412 (2001) 169–172.
[19] J. Qi, L.H. Jiang, S.L. Wang, G.Q. Sun, Applied Catalysis B: Environmental 107 (2011) 95–103.
[20] J.B. Joo, Y.J. Kim, W.Y. Kim, P. Kim, J.H. Yi, Catalysis Communications 10 (2008) 267–271.
[21] M. Sevilla, C. Sanchis, T. Valdes-Solis, E. Morallon, A.B. Fuertes, Carbon 46 (2008) 931–939.
[22] S. Aikawa, T. Kizu, E. Nishikawa, Carbon 48 (2010) 2997–2999.
[23] Y. Ando, X.L. Zhao, S. Inoue, S. Iijima, Journal of Crystal Growth 237–239 (2002) 1926–1930.
[24] D.H. Jurcakova, X. Li, Z.H. Zhu, R.D. Marco, G.Q. Lu, Energy Fuel 22 (2008) 4139–4145.
[25] M. Sevilla, C. Sanchis, T. Valdes-Solis, E. Morallon, A.B. Fuertes, Journal of Physical Chemistry C 111 (2007) 9749–9756.
[26] D.S. Yuan, X.L. Yuan, W.J. Zou, F.L. Zeng, X.J. Huang, S.L. Zhou, Journal of Materials Chemistry 22 (2012) 17820–17826.
[27] Z.M. Sheng, J.N. Wang, Advanced Materials 20 (2008) 1071–1075.
[28] J.H. Bang, Electrochimica Acta 56 (2011) 8674–8679.
[29] L. Zhang, F. Li, Applied Clay Science 50 (2010) 64–72.
[30] J. Das, B.S. Patra, N. Baliarsingh, K.M. Parida, Applied Clay Science 32 (2006) 252–260.
[31] Z.X. Yu, D. Chen, M. Ronning, T. Vralstad, E.O. Fernández, A. Holmen, Applied Catalysis A: General 338 (2008) 136–146.
[32] S. Pradhan, F.R. Costa, U. Wagenknecht, D. Jehnichen, A.K. Bhowmick, G. Heinrich, European Polymer Journal 44 (2008) 3122–3132.
[33] Y. Tian, G. Wang, F. Li, D.G. Evans, Materials Letters 61 (2007) 1662–1666.
[34] Z.L. Wang, X.B. Zhang, X.J. Liu, M.F. Lv, K.Y. Yang, J. Meng, Carbon 49 (2011) 161–169.
[35] A. Sadezky, H. Muckenhuber, H. Grothe, R. Niessner, U. Poschl, Carbon 43 (2005) 1731–1742.
[36] J.B. Joo, Y.J. Kima, W.Y. Kima, P. Kim, J.H. Yi, Catalysis Communications 10 (2008) 267–271.
[37] L.S. Zhang, W. Li, Z.M. Cui, W.G. Song, Journal of Physical Chemistry C 113 (2009) 20594–20598.
[38] K.S.W. Sing, D.H. Everett, R.A.W. Haul, L. Moscou, R.A. Pierotti, J. Rouquerol, T. Siemieniewska, Pure and Applied Chemistry 157 (1985) 603–619.
[39] M.D. Hawley, S.V. Tatawawadi, S. Piekarski, R.N. Adarns, Journal of the American Chemical Society 89 (1967) 447–450.
[40] M. Kudera, Y. Nakagawa, S. Fletcher, H.A.O. Hill, Lab on a Chip 2 (2001) 127–131.
[41] M. Zhou, Y.M. Zhai, S.J. Dong, Analytical Chemistry 81 (2009) 5603–5613.
[42] J.P. Dong, Y.Y. Hu, J.Q. Xu, X.M. Qu, C.J. Zhao, Journal of Electroanalytical Chemistry 21 (16) (2009) 1792–1798.
[43] K. Nakano, K. Ohkubo, H. Taira, M. Takagi, N. Soh, T. Imato, Journal of Electroanalytical Chemistry 623 (2008) 49–53.
[44] D. Nematollahi, H. Shayani-Jam, M. Alimoradi, S. Niroomand, Electrochimica Acta 54 (2009) 7407–7415.
[45] H.L. Qi, C.X. Zhang, Journal of Electroanalytical Chemistry 17 (10) (2005) 832–838.
[46] M.G. Li, F. Ni, Y.L. Wang, S.D. Xu, D.D. Zhang, S.H. Chen, L. Wang, Journal of Electroanalytical Chemistry 21 (2009) 1521–1526.